A Tsuji Burner in a Counterflow

Brandon Li, Antonio L. Sánchez, Forman. A. Williams
University of California San Diego
La Jolla, CA, USA

1 Introduction

Tsuji burners have been used extensively by the combustion community for over 50 years [1]. The flame is established in the forward stagnation-point region of a porous cylinder of radius a placed in a uniform air stream, with the fuel released by injection perpendicular to the cylinder surface with velocity U_i. For sufficiently small injection velocities, the flame develops along the boundary layer that is established on the cylinder surface, with the solution found around the forward stagnation point exhibiting a well-known selfsimilar structure determined by the value of the local strain rate exerted by the outer stream [2]. Higher injection velocities lead to boundary-layer blowoff, a case investigated recently [3].

Recent numerical work [4] has considered a modification to the basic Tsuji burner in which the porous cylinder is placed instead at the center of a planar air counterflow with strain rate A_∞, a configuration schematically represented in Figure 1. The proposed design, providing increased oxidizer feed to the diffusion flame, enables the investigation of transition from the counterflow flame found near the centerline stagnation point to the planar-jet flame developing along the symmetry plane. The previous study considered in particular the case of a weak counterflow, corresponding to small values of the Reynolds number $Re = A_\infty a^2/\nu$, with ν representing the air value of the kinematic viscosity. To simplify the analysis, the velocity was taken to be that of the potential solution, obtained by combining the stagnation-point flow with a line source and a quadrapole of appropriate strength. Since the potential solution includes a tangential component on the cylinder surface, it is in principle incompatible with the condition that fuel is injected perpendicular to the wall, that being the condition most often found in applications. This deficiency of the model was found to have a limited effect for the specific case of weak counterflow analyzed in [4], for which vorticity remains relatively small.

The present analysis revisits the problem by considering the limit of moderately large Reynolds numbers $Re \gg 1$, applicable to most experimental burners. Specific attention is given to configurations with fuel-injection velocities U_i comparable in magnitude to the characteristic counterflow velocity $A_\infty a$, so that the boundary layer is blown off the cylinder surface, with the result that mixing and chemical reaction are confined to two twin mixing layers of characteristic thickness $\delta = a/Re^{1/2}$ separating the fuel from the air on opposite sides of the counterflow. Outside these mixing layers the flow is inviscid. The flow in the air stream is irrotational everywhere, whereas on the fuel side the flow is rotational, with the vorticity along each streamline determined by its value at the injection location. Since in the inviscid limit the temperature and composition also remain constant along streamlines, the problem reduces to one

Correspondence to: als@ucsd.edu

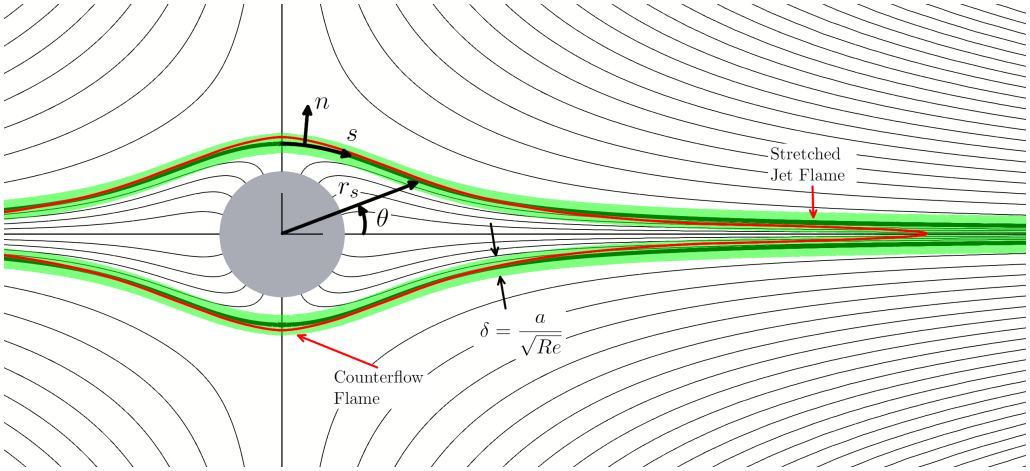

Figure 1: The flow configuration investigated here, with streamlines corresponding to the case $\Lambda = 1$.

involving constant density on the air and fuel sides. As shown in [5,6] for the case of two opposing jets, introduction of density-weighted kinematic variables effectively reduces the problem to one involving two streams of equal density, thereby removing the vortex-sheet character of the interface. Transformations utilizing density-weighted variables are commonly used in the analysis of steady stratified flows (see, e.g. [7] and references therein). The resulting streamfunction-vorticity formulation, adopted for instance in our recent investigation of Tsuji burners with augmented fuel injection [3], is to be employed below to analyze porous cylindrical burners in counterflows for varying levels of fuel injection. The numerical integrations reveal, in particular, that the differences from the potential solution are largest for weak injection, whereas for strong injection the potential solution remains fairly accurate, in agreement with the previous numerical results [4]. The computation of the inviscid flow provides the distribution of strain rate acting along the mixing layer, which in turn determines the structure of the diffusion flame.

2 Formulation

The inviscid flow will be described in cylindrical coordinates, the radial distance r from the cylinder center being scaled with the cylinder radius a and the azimuthal angle θ measured from the plane separating the counterflow streams, as indicated in Figure 1, where $r_s(\theta)$ represents the interface separating the air and fuel regions, to be determined as part of the computation. Because of the existing symmetry, it suffices to give the solution in the quadrant $0 \leq \theta \leq \pi/2$. The radial and azimuthal velocity components will be scaled with $A_\infty a$ to give the dimensionless variables v_r and v_θ, which take the values $v_r = r\cos(2\theta)$ and $v_\theta = -r\sin(2\theta)$ in the approaching counterflow and $v_r = \Lambda = U_i/(A_\infty a)$ and $v_\theta = 0$ on the cylinder surface. For simplicity, the problem is initially formulated for cases in which the fuel density ρ_F is equal to the air density ρ_A; the minor modifications needed to extend the formulation to cases with $\rho_F \neq \rho_A$ are discussed below, following ideas developed earlier [5,6].

The problem will be formulated conveniently in terms of the dimensionless stream function ψ, defined such that

$$v_r = \frac{1}{r}\frac{\partial \psi}{\partial \theta} \quad \text{and} \quad v_\theta = -\frac{\partial \psi}{\partial r}. \tag{1}$$

For the planar flow investigated here, the equation for the vorticity

$$\omega = \frac{1}{r}\frac{\partial}{\partial r}(r v_\theta) - \frac{1}{r^2}\frac{\partial v_r}{\partial \theta}, \tag{2}$$

reduces to

$$v_r \frac{\partial \omega}{\partial r} + \frac{v_\theta}{r} \frac{\partial \omega}{\partial \theta} = 0, \tag{3}$$

indicating that the vorticity is conserved along streamlines, so that $\omega = \omega(\psi)$. Use of (1) in (2) provides

$$\frac{1}{r} \frac{\partial}{\partial r} \left(r \frac{\partial \psi}{\partial r} \right) + \frac{1}{r^2} \frac{\partial^2 \psi}{\partial \theta^2} = -\omega(\psi), \tag{4}$$

as a Poisson equation for ψ with an unknown nonlinear source function $\omega(\psi)$. The above equation must be integrated for $1 \leq r < \infty$ and $0 \leq \theta \leq \pi/2$ subject to the boundary conditions

$$\begin{cases} \psi - \Lambda\,(\theta - \pi/2) = \partial\psi/\partial r = 0 & \text{at } r = 1 & \text{for } 0 \leq \theta \leq \pi/2 \\ \psi = 0 & \text{at } \theta = \pi/2 & \text{for } 1 \leq r < \infty \\ \psi \to (r^2/2)\sin(2\theta) & \text{as } r \to \infty & \text{for } 0 < \theta \leq \pi/2 \\ \psi = -(\pi/2)\Lambda & \text{at } \theta = 0 & \text{for } 1 \leq r < \infty \end{cases} \tag{5}$$

where the arbitrary value of ψ along the separating streamline $r = r_s(\theta)$ has been selected to be $\psi = 0$, with the air/fuel sides corresponding to positive/negative values of ψ, respectively. The far-field solution is dominated by the streamfunction $\psi = (r^2/2)\sin(2\theta)$ of the counterflowing solution, with corresponding horizontal and vertical velocity components

$$\begin{cases} v_x = v_r \cos\theta - v_\theta \sin\theta = x \\ v_y = v_r \sin\theta + v_\theta \cos\theta = -y \end{cases}, \tag{6}$$

with $x = r\cos\theta$ and $y = r\sin\theta$. Since $\psi = \Lambda\,(\theta - \pi/2)$ on the cylinder surface, the function $\omega(\psi)$, to be determined as part of the numerical integration, is related to the distribution of vorticity on the cylinder wall $\Omega(\theta)$ by

$$\omega = \begin{cases} 0 \quad \text{for } \psi \geq 0 \\ \Omega(\psi/\Lambda + \pi/2) \quad \text{for } -\pi\Lambda/2 \leq \psi \leq 0 \end{cases}. \tag{7}$$

As can be seen, the above formulation depends only on the rescaled injection velocity $\Lambda = U_i/(A_\infty a)$. As shown earlier [5, 6], the analysis of configurations where the fuel-stream density ρ_F differs from the air density ρ_A requires incorporation of a scaling factor $(\rho_F/\rho_A)^{1/2}$ in the definition of the vorticity and fuel-side stream function. In terms of these rescaled variables, the formulation reduces exactly to that given above in (4) and (5), with the parameter $\Lambda = (\rho_F/\rho_A)^{1/2} U_i/(A_\infty a)$ representing in this case a density-square-root-weighted injection velocity.

Numerical integration is needed to solve (4) subject to (5). The function $\omega(\psi)$ is uniquely determined by the condition that fuel injection is perpendicular to the fuel surface, i.e. $\partial\psi/\partial r = 0$ at $r = 1$, with other fuel-injection conditions resulting in different vorticity distributions. For example, the potential solution

$$\psi_p = \frac{1}{2}\left(r^2 - \frac{1}{r^2}\right)\sin(2\theta) + \Lambda\left(\theta - \frac{\pi}{2}\right), \tag{8}$$

adopted in the previous investigation [4] as an approximate description for the velocity field, involves an azimuthal velocity component $v_\theta = -2\sin(2\theta)$ on the cylinder surface, additional to the uniform radial component $v_r = \Lambda$. Although such a velocity distribution conceivably could be achieved in experiments by varying simultaneously the injection angle and the speed along the cylinder surface, the required experimental arrangement would be difficult.

3 Representative numerical results

The numerical integration of (4) with boundary conditions (5) employs an iterative scheme involving the computation of the rotational component of the streamfunction $\psi_r = \psi - \psi_p$, which must satisfy also a Poisson equation. The rotational component ψ_r is identically zero on all boundaries, but its radial gradient satisfies the inhomogeneous boundary condition $\partial\psi_r/\partial r = 2\sin(2\theta)$ at $r = 1$, as needed to achieve normal fuel injection. The procedure is initialized by guessing the unknown vorticity distribution on the cylinder surface $\Omega(\theta)$ and integrating the associated Poisson equation for ψ_r subject to homogeneous boundary conditions. The resulting slip velocity $\partial\psi_r/\partial r$ at $r = 1$ is in general different from the target value $\partial\psi_r/\partial r = 2\sin(2\theta)$. The difference between both was utilized to update the distribution $\Omega(\theta)$ to be used in the subsequent iteration. The procedure was repeated until convergence to the desired solution was achieved.

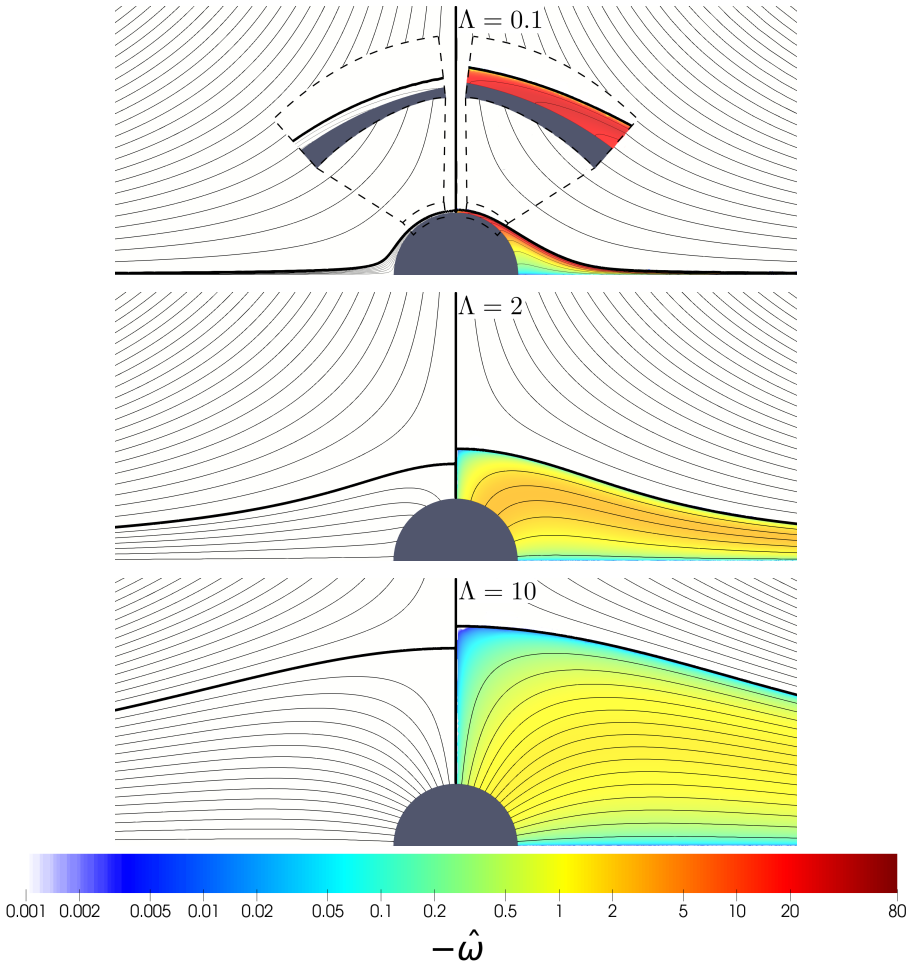

Figure 2: The right half of each panel represents the streamlines and vorticity distribution corresponding to different values of Λ obtained by integration of (4) with boundary conditions (5). The left half shows the streamlines of the corresponding potential flow, evaluated with use made of (8). The spacing used for the stream function is $\delta\psi = 1$ on the air side $\psi > 0$ and $\delta\psi = (0.02, 0.5, 1)$ for $\Lambda = (0.1, 2, 10)$ on the fuel side $\psi < 0$.

Results of sample integrations for selected values of Λ are presented in Figure 2. The plots show streamlines and accompanying vorticity distributions, the latter represented by color contours. The interface $r = r_s(\theta)$ separating the fuel and air regions, corresponding to the streamline $\psi = 0$, departs from the

stagnation point, located at $r = r_s(\pi/2)$, and develops sideways, forced by the counterflowing stream. As expected, the numerical solutions show that the stagnation point moves farther from the surface with increasing injection velocity.

The vorticity is very large for small injection, because of the large spin associated with the rapid streamline deflection occurring near the cylinder surface, illustrated in the right-hand-side inset for $\Lambda = 0.1$, to be compared with the potential-flow case, whose straight streamlines form a small angle with the cylinder surface, as shown in the left-hand-side inset of the same figure. As is to be expected, the vorticity is moderately small for large injection, when the streamlines remain aligned in the radial direction, as shown in the results for $\Lambda = 10$. This is further quantified in Figure 3, which shows wall vorticity distributions $\Omega(\theta)$ for different values of Λ, as well as asymptotic predictions, to be discussed below.

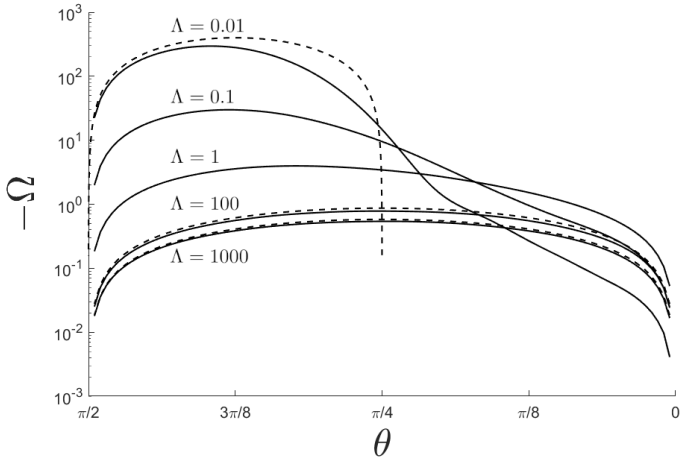

Figure 3: The solid curves represent the function $\Omega(\theta)$ obtained numerically by integration of (4) with boundary conditions (5) for selected values of Λ. The dashed curves represent the asymptotic predictions for $\Lambda \ll 1$ (evaluated at $\Lambda = 0.01$) and for for $\Lambda \gg 1$ (evaluated at $\Lambda = 100$ and $\Lambda = 1000$).

To illustrate the effects of vorticity on the resulting flow Figure 2 shows also the streamlines corresponding to the potential solution (8) and its associated fuel-air interface

$$r_s = \left\{ \sqrt{1 + \left[\frac{(\pi/2 - \theta)\Lambda}{\sin(2\theta)} \right]^2} + \frac{(\pi/2 - \theta)\Lambda}{\sin(2\theta)} \right\}^{1/2} \tag{9}$$

the latter obtained by setting $\psi_p = 0$ in (8). As expected, for $\Lambda = 10$, when vorticity production at the porous-wall surface is limited, the differences with the potential solution are fairly small, but they become more noticeable for small injection velocities, especially on the fuel side. For $\Lambda = 0.1$ it can be seen that the separating streamline $\psi = 0$ of the potential flow remains close to the cylinder surface, while that of the rotational solution separates at $\theta \simeq \pi/4$ to form a detached vortex sheet bounding a low-velocity cavity. From a fundamental viewpoint, it is of interest that the inviscid flow with negligibly small injection velocity does not approach the potential flow solution, but rather adopts a cavity structure, reminiscent of the idealized wake flows envisioned by Kirchhoff [8].

4 Additional work

In work not shown here, asymptotic methods have been used to investigate the form of the solution for extreme values of Λ. In the limit $\Lambda \ll 1$ of weak injection, the vorticity, scaling with Λ^{-1}, is confined to

a thin near-cylinder boundary layer of thickness Λ that necessarily separates from the cylinder to form a cavity of finite size on both sides of the cylinder. In the opposite limit $\Lambda \gg 1$ of strong injection, the vorticity needed to maintain the fuel flow normal to the porous cylinder is found to be small, of order $1/\ln\Lambda \ll 1$, so that the flow is irrotational in the first approximation. The velocity distribution along the fuel-air interface is seen to determine the evolution of the diffusion flame, including the length of the stretched jet flames that develops along the counterflow center plane.

5 Conclusions

A Tsuji burner in a counterflow, with moderately large Reynolds numbers based on the cylinder diameter and the counterflow strain rate, exhibits a rich variety of fluid-dynamical phenomena that can be described well by asymptotic methods. In particular, the flow fields are quite different for large and small ratios of the injection velocity to the counterflow velocity. The configuration offers the possibility of investigating both counterflow flame structures and (previously unexplored) stretched-jet-flame structures in the same test facility. It could be of interest to pursue experimental investigations of this type.

References

[1] H. Tsuji and I. Yamaoka, *The counterflow diffusion flame in the forward stagnation region of a porous cylinder*, Proc. Combust. Inst. 11 (1967), pp. 979–984.

[2] H. Tsuji, *Counterflow diffusion flames*, Prog. Ener. Combust. Sci. 8 (1982), pp. 93–119.

[3] B. Li, J. Graña, A.L. Sánchez, and F.A. Williams, *Aerodynamics of tsuji burners with augmented fuel injection*, Combust. Sci. Technol. submitted (2021), p. .

[4] M.P. Severino, M.S. Donini, and F.F. Fachini, *Dynamics of diffusion flames in a very low strain rate flow field: from transient one-dimensional to stationary two-dimensional regime*, Combustion Theory and Modelling 25 (2021), pp. 861–888.

[5] J. Carpio, A. Liñán, A.L. Sánchez, and F.A. Williams, *Aerodynamics of axisymmetric counterflowing jets*, Combust. Flame 177 (2017), pp. 137–143.

[6] A. Weiss, W. Coenen, and A. Sánchez, *Aerodynamics of planar counterflowing jets*, J. Fluid Mech. 821 (2017), pp. 1–30.

[7] C.S. Yih, *Vortices and vortex rings of stratified fluids*, SIAM J. Appl. Math. 28 (1975), pp. 899–912.

[8] T.Y.T. Wu, *Cavity and wake flows*, Annu. Rev. Fluid Mech. 4 (1972), pp. 243–284.